Energy Conversion and Management 119 (2016) 422–434

Contents lists available at ScienceDirect

Energy Conversion and Management

journal homepage: www.elsevier.com/locate/enconman

Exergoeconomic analysis and multi objective optimization of performance of a Carbon dioxide power cycle driven by geothermal energy with liquefied natural gas as its heat sink

Mohammad H. Ahmadi [a], Mehdi Mehrpooya [a,b,*], Fathollah Pourfayaz [a]

[a] Department of Renewable Energies and Environmental Eng, Faculty of New Sciences and Technologies, University of Tehran, Tehran, Iran
[b] Hydrogen and Fuel Cell Laboratory, Faculty of New Sciences and Technologies, University of Tehran, Tehran, Iran

ARTICLE INFO

Article history:
Received 30 January 2016
Received in revised form 13 April 2016
Accepted 18 April 2016
Available online 26 April 2016

Keywords:
Exergoeconomic
Carbon dioxide cycle
Liquefied natural gas
Exergy analysis

ABSTRACT

In this study a transcritical Carbon dioxide power cycle has been coupled to a liquefied natural gas to work either as the cold source and to further enhance to generate electricity. The detailed thermodynamic analysis is performed in order to investigate the effect of key parameters on the cycle performance. Also, heat exchangers are measured to find the heat transfer surface area for economic evaluation. To investigate the aforementioned cycle and for optimization purposes, an exergoeconomic analysis is done to know the important components with respect to exergoeconomic criterion. The exergoeconomic analysis reveals that Carbon dioxide turbine and condenser have the highest rate of sum cost rate associated with capital investment and the cost of exergy destruction and special attention should be paid to these components. The parametric analysis shows that there is an optimum turbine inlet pressure which brings about the highest exergy efficiency and lowest product cost rate. Moreover, the condensate pressure has the highest effect on system exergy efficiency compared to others. With the help of multi-objective optimization, the cumulative effects of these variables are investigated on the system to maximize the exergetic efficiency and to minimize the product cost rate of the system. Results show that the system is capable of producing power with exergy efficiency and product cost rate equal to 20.5% and 263592.15 $/year, respectively, according to technique for order of preference by similarity to ideal solution decision making technique. Also, the system exergy efficiency of 22.1% and 295001.26 $/year product cost rate is achieved through linear programming techniques for multidimensional analysis of preference technique and 23.97% exergy efficiency and 370378.758 $/year product cost rate is given with FUZZY decision making technique.

1. Introduction

An enduring area of interest for engineers, in which lots of work has been performed, is the conversion of heat to electricity. Recently, there is growing interest in utilizing low and moderate temperature heat sources, which are available via solar, geothermal and biogenic energy systems, and as waste heat from industries. For producing power, one can consider such cycles as ORCs (organic Rankine cycles) [1–10], Kalina cycles [13–17] and trilateral cycles (TLCs) [18,19].

DiPippo [2] compared the ORC and the Kalina geothermal plant through the second law of thermodynamics and suggested an approach to evaluate the plant efficiencies with analogous environmental settings and inputs. Tchanche and colleagues [3] demonstrated several uses of organic Rankine cycles as a tool for power generation by employing low grade heat. Saleh and colleagues [4] investigated the thermodynamic performances of 31 pure working fluids for organic Rankine cycles on the basis of the BACKONE equation of state. Properties of a good fluid are: high efficiency, low specific volumes, low cost, moderate pressures in the heat exchangers, low ODP, low toxicity and low GWP among others. Maizza and Maizza [5], Badr and colleagues [6] are some of the scholars who investigated the features of various working fluids in view of their selection in an ORC use. Hettiarachchi et al. presented a cost-effective optimum design criterion for ORCs utilizing low temperature geothermal heat sources. The optimum cycle performance was compared for various working fluids including ammonia, HCFC123, n-Pentane, and PF5050 [7]. Drescher

* Corresponding author at: Department of Renewable Energies and Environmental Eng, Faculty of New Sciences and Technologies, University of Tehran, Tehran, Iran.
E-mail address: mehrpoya@ut.ac.ir (M. Mehrpooya).

http://dx.doi.org/10.1016/j.enconman.2016.04.062
0196-8904/

Nomenclature

T	temperature (K)
W	power (kW)
m	mass flow (kg/s)
Cp	specific heat (kJ/kg K)
TIP	turbine inlet pressure
TIT	turbine inlet temperature
p	pressure (bar)
h	specific enthalpy (kJ/kg)
E	exergy (kW)
e	specific exergy (kJ/kg)
Q	heat (kW)
s	specific entropy (kJ/kg K)
Z	capital cost rate ($/year)
c	cost per unit exergy ($/GJ)
C	flow cost rate ($/year)
i	inlet
o	outlet
0	ambient condition
ph	physical
ch	chemical
H	plant life time (year)
A	area (m^2)
U	total heat transfer coefficient
r	relative cost difference (%)
f	exergoeconomic factor (%)

Greek symbol

η	exergy efficiency

Subscript

HX	heat exchanger

and Bruggemann [8] developed software to find thermodynamically suitable fluids for ORC in biomass power and heat plants. Yamamoto et al. designed an ORC by using an electric evaporator instead of an external heat source. R123 and water were used as the working fluids and experiments were conducted to compare each fluid. Its maximum cycle efficiency and electric power were shown to be 1.25% and 150 W, respectively [9]. Zhang and colleagues [10] evaluated the economic and thermodynamic performance for low-temperature geothermal power plant of both transcritical and subcritical ORC power cycle systems. Various researches have been carried out to study the Kalina cycle, which was originally considered by Kalina [11]. El-Sayed and Tribus [12] conduct a theoretic evaluation of the Kalina cycle with Rankine cycle. The arrangements proposed by them were very much complex owing to a number of heat exchangers had more than two steams. Ashouri et al. [13] performed an exergy analysis on a Kalina cycle driven by Trough collector. Marston [14] carried out the parametric analysis of the Kalina cycle. He suggested an approach of settling the Kalina cycle and recognized the main variables for optimizing the Kalina cycle. Rogdakis [15] suggested formulas explaining the optimal operation of the Kalina cycle. Marston [16] evaluated the Kalina cycle with triple pressure. He found that Kalina cycle was more effective than the triple pressure steam cycle. Zamfirescu and Dincer [18] analyzed trilateral ammonia–water Rankine cycle that uses no boiler, but rather the saturated liquid is flashed by an expander. Fischer [19] found that exergy efficiency for power production is higher by 14–29% for the TLC with the two-phase expander utilization in comparison to the ORC. Exploitation of renewable energy has become an important topic due to the energy shortage and growing carbon dioxide emissions. Although the organic Rankine cycle systems, which contain lower boiling temperature working fluids, have great advantages and suitability for utilizing low-temperature heat source to produce useful power [20–22], there is a pinch point occurred between working fluid and heat source in a constant temperature boiling process of a pure fluid. In additional, with the development of the Kalina cycle for geothermal energy and waste heat applications, turbines with NH_3–H_2O as working fluid are existing technologies. There have been some commercial power plants using NH_3–H_2O for geothermal energy or industrial waste heat, such as Husavik plant in Iceland, Unterhaching plant in Germany, and several plants in Japan [20]. The technical feasibility of ORC application in general low-grade heat utilization has already been investigated and validated [21]. This minimal temperature difference results in a largest resistance in heat transfer and causes a significant destruction in energy conversion [23]. Chen et al. [23] implemented a thorough reasonable investigation for low-grade heat conversion between a R32-based and a CO_2-based transcritical Rankine cycle by exergy and energy analysis. Walraven and colleagues [24] studied the low-temperature geothermal sources by optimizing and investigating the performance of various groups of Kalina and ORC cycle.

Various studies were carried on the supercritical and transcritical CO_2 power generation cycles. Velez and colleagues [25] compared and investigated a CO_2 transcritical power cycle without and with an internal heat exchanger. Wang and colleagues [26] carried out an exergy analysis and a parametric analysis for supercritical CO_2 power cycle besides they made attempt to optimize the exergy efficiency via ANN and genetic algorithm (GA). Baik and colleagues [27] compared and optimized the power output between a R125 transcritical cycle and a CO_2 transcritical cycle for the exploitation of low-grade heat source of about 100 °C. Lakew and colleagues [6] by employing low temperature heat source and substitution the mechanical pump by a thermal driven pump, the performance of a supercritical CO_2 Rankine cycle enhanced.

Lin and colleagues [28] studied a transcritical CO_2 Rankine cycle which employed the liquefied Natural Gas (LNG) firstly as heat sink. Gao and colleagues [29] suggested two new light hydrocarbon separation processes via employing the cryogenic energy of LNG. Mehrpooya et al. [30] has investigated a novel integrated air separation processes, cold energy recovery of liquefied natural gas and carbon dioxide power cycle. Wang and colleagues [31] conducted a MOEA and a thermodynamic analysis for an ammonia-water power system works with LNG as heat sink. Song and colleagues [32] used the LNG to cool the exhausted gas from the turbine in a solar-driven transcritical CO_2 power cycle. Few of these aforementioned researches has conducted a MOEA for the supercritical or transcritical CO_2 power generation system with LNG as heat sink and carried out the performance analysis from the economical point of view.

In recent years, exergoeconomic concept has been applied in power plants and CCHP system analyses [33–44]. A techno-economic analysis of a ground heat pump system was carried out by Esen and colleagues [33]. Also they compared it with traditional heating system. From economic and efficiency viewpoints, the suggested heat pump system is valuable, except for natural gas. Esen and colleagues [34] implemented the same evaluations on horizontal ground heat pump systems. The outcomes of their analyses reveal that for a heat pump system at the depth of two meters the

exergy efficiency and Coefficient of performance (COP) are 56.3% and 2.8%, correspondingly. Moreover, increasing the heat source temperature has a positive influence on exergy efficiency and COP. Techno-economic analysis is a powerful means to appraise the economic and thermodynamic performance of energy systems and has gained much attention by various scholars. Esen and colleagues [35] carried out a thorough evaluation of two heat pump systems. They designed ground-coupled and air-coupled heat pumps and evaluated the two systems experimentally. The average cooling performance of air-coupled heat pump system was found to be 3.17 which were lower than that of ground-coupled system (3.85 and 4.26 for 1 and 2 m depth, correspondingly). Also, the ground-coupled system is economically preferable to air-coupled system.

Temir and Bilge [36] applied thermoeconomic method for a trigeneration system with reciprocating engine as a prime mover. They also investigated the variation of unit exergetic cost of products with unit energy cost of natural gas and found that absorption chiller unit was more sensitive to this variation. They suggested this method to be used for complicated systems in order to make necessary improvements in the system performance. Kong et al. [37] investigated the energy efficiency and economic feasibility of a CCHP driven by Stirling engine and showed that the price of the natural gas as a fuel of Stirling engine plays an important role in economic feasibility of system and payback period decreases as the price of natural gas increases. Huangfu et al. [38] evaluated a micro-scale combined cooling, heating and power system (MCCHP) in a view of energy, exergy and economy. Economic analysis showed that with the present price of the natural gas, the payback time is 2.97 years. In addition, to have an efficient system, electricity output should be more than half of the load.

Exergoeconomic analysis is used for single mixed refrigerant natural gas liquefaction processes and sensitivity of exergy destruction cost and exergoeconomic factor to operating variables are studied [39]. They formulated system components from the view point of thermoeconomic analysis. The same authors, in part II of [40], of this paper applied the methodology of the first part to the mentioned system. In this paper, they carried out thermodynamic modeling and modeled the system by exergoeconomic principles. They also calculated the specific unit of exergetic cost of electrical power, chilled water and heating energy produced by this trigeneration system. Al-Sulaiman et al. [41] applied exergoeconomic analysis to thermoeconomically model three trigeneration systems such as SOFC-trigeneration, biomass-trigeneration and solar-trigeneration. They also conducted thermoeconomic optimization using Powell's direct research method to minimize the product cost rate of these three systems. The same authors, in part II of [42] discussed the results of exergy and thermoeconomic modeling of these three systems and showed that SOFC-trigeneration had the highest exergy efficiency and the lowest cost per exergy unit while solar trigeneration had the lowest exergy efficiency and the highest cost per exergy unit among these three systems. Advanced exergoeconomic evaluation of single mixed refrigerant natural gas liquefaction processes are studied [43]. Advanced Exergoeconomic analysis is used for multistage mixed refrigerant natural gas liquefaction processes and sensitivity of exergy destruction cost and exergoeconomic factor to operating variables are studied [44].

Multi-objective optimization is a great asset for solving engineering issues [45–47]. Özyer and colleagues [45] evolved an intellectual model for prospect calculation by using of evolutionary algorithms. The multi-objective optimization is performed by various engineering issues such as vehicle routing problems with Time Windows [46]. Blecic and colleagues [47] illustrated a decision support system called Bay MODE on the basis of multi-objective optimization and Bayesian analysis.

Answering a multi-objective issue for the paramount execution is a hard assignment for the reason that it requires instantaneous fulfillment of different and occasionally conflicting objective functions. For answering such problems, various approaches including evolutionary algorithms (EA) was introduced in 20th century to help some multi-objective issues [48,49]. The output of multi-objective optimization will be a series of answers named Pareto frontier which illustrates realistic answers in the objective area. Multi-objective optimization method was commonly employed in energy systems engineering exponentially [49–57]. Ahmadi et al. [50,51] developed an intelligent approach to figure power of solar Stirling heat engine by implementation of evolutionary algorithms. Ahmadi et al. [52] applied non dominated sorting genetic algorithm for thermo-economic optimization of solar driven heat engine. Ahmadi et al. [53] applied non dominated sorting genetic algorithm for thermo-economic optimization of Stirling heat pump. Sayyaadi et al. [54] applied non dominated sorting genetic algorithm for optimal design of a Solar-Driven Heat Engine. Ahmadi and colleagues [55] carried out multi-objective optimization and thermodynamic analysis of an irreversible three-heat-source absorption heat pump.

Sadatsakkak and colleagues [56] carried out multi-objective optimization and thermo-economic analysis of an irreversible regenerative closed Brayton cycle. Sadatsakkak and colleagues [57] carried out multi-objective optimization and thermodynamic analysis of an endoreversible Braysson cycle.

In this paper, transcritical carbon dioxide cycle has been coupled with liquefied natural gas process and geothermal water as the cold sink and warm source, respectively. Following works are performed on the investigated cycle:

- By means of exergoeconomic criterion, the system performance is evaluated in detail in terms of exergetic and economic criteria.
- Effects of key parameters including turbine inlet temperatures and pressures, condensate pressure and LNG pressure are investigated on work output, exergy efficiency and product cost rate along with ecological coefficient of performance (ECOP).
- The system has been optimized with respect to exergy efficiency and product cost rate and ECOP using genetic algorithm with four decision variables.
- Different decision making techniques are investigated and compared on the obtained results.

2. System description

Fig. 1 shows the scheme of the transcritical CO_2 geothermal power generation system via the cold energy exploitation of LNG. The deep underground geothermal water is employed and transported to the evaporator. The geothermal water is then re-injected to the underground later discharging a huge value of heat. For pressurizing the liquid CO_2 from condenser to the supercritical condition the supporter pump (booster) I is employed. To gain the heat and produce high pressure and high temperature supercritical CO_2 vapor, this liquid CO_2 then pass in the evaporator. The supercritical CO_2 vapor expands via CO_2 turbine to push the electrical producer to generate electrical energy. Again the exhausted gas from the CO_2 turbine is cooled to be liquid in the condenser. To promote LNG pressure to a supercritical pressure the LNG in the storage tank pressurized initially via the booster pump II, and then plays role of a heat sink in the condenser to cool the exhausted gas from the CO_2 turbine. To rise the temperature of the heated natural gas, it continuously enters the heater and absorbs heat from environmental water. To generate electrical energy the high pressure heated natural gas expands by a natural gas turbine. Finally, the exhausted natural gas from the natural

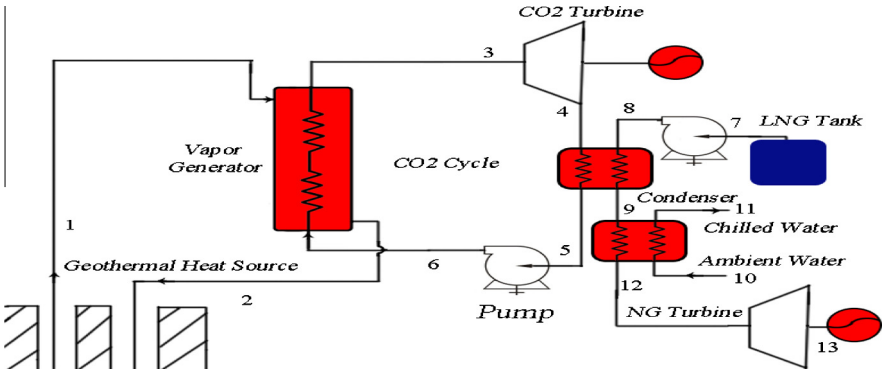

Fig. 1. Graphical illustration of the geothermal power generation system.

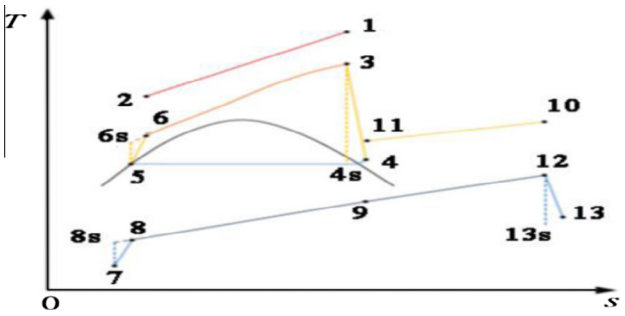

Fig. 2. T–s plot for the system of the geothermal power production [62–64].

gas turbine is transferred to the natural gas receiving station to propose natural gas to the consumers.

Fig. 2 demonstrates T–s plot for the system of the geothermal power generation. The main advantage of this process is using cold energy of LNG to reduce the back pressure of CO_2 turbine which results increasing in the output power of the CO_2 turbine. Furthermore, the natural gas heated using the environmental water expanding via the NG turbine also improves the output power of the entire system. The system of electrical energy production could gain better efficiency of energy conversion.

3. Mathematical approaches and performance indexes

3.1. Mathematical approaches

In order to simplify the mathematical approach of the whole system, following assumptions were considered:

(1) The system works under steady state circumstances.
(2) The heat transfer between the environment and the equipment of the system is ignored.
(3) The CO_2 at the condenser outlet is saturated liquid.
(4) The pressure changes throughout the pipe assemblies are ignored.
(5) A constant pressure drop equal to 5% is assumed for heat exchangers including condenser, heater and vapor generator.
(6) A constant isentropic efficiency of 80% is assumed for turbines and pumps.

The aforementioned system is generally included four types of equipment including turbine, heat exchanger, pump and condenser. As stated by the energy and mass conversation laws, the mathematical model of each element can be determined as following as:

$$m_1(h_1 - h_2) = m_{CO_2}(h_3 - h_6) \quad (1)$$

$$m_{LNG}(h_9 - h_{12}) = m_w(h_{10} - h_{11}) \quad (2)$$

A non-isentropic expansion process occurs throughout the turbines (NG turbine and CO_2 turbine) that expressed using the isentropic efficiency as below:

$$\eta_{tb.CO_2} = \frac{h_3 - h_4}{h_3 - h_{4s}} \quad (3)$$

$$\eta_{tb.NG} = \frac{h_{12} - h_{13}}{h_{12} - h_{13s}} \quad (4)$$

The output power produced using the turbines are formulated as below:

$$W_{tb,CO_2} = m_{CO_2}(h_3 - h_4) \quad (5)$$

$$W_{tb,NG} = m_{LNG}(h_{12} - h_{13}) \quad (6)$$

The energy balance in the condenser can be written as following as:

$$m_{LNG}(h_8 - h_9) = m_{CO_2}(h_4 - h_5) \quad (7)$$

The isentropic efficiency for the booster pump I and II can be written as below:

$$\eta_{Pump,I} = \frac{h_{6s} - h_5}{h_6 - h_5} \quad (8)$$

$$\eta_{Pump,II} = \frac{h_{8s} - h_7}{h_8 - h_7} \quad (9)$$

The pumps' power consumption can be written as follow:

$$W_{Pump,I} = m_{CO_2}(h_6 - h_5) \quad (10)$$

$$W_{Pump,II} = m_{LNG}(h_8 - h_7) \quad (11)$$

The net output power of the system can be obtained as below:

$$W_{net} = W_{tb,CO_2} + W_{tb,NG} - W_{Pump,I} - W_{Pump,II} \quad (12)$$

Specifically near critical point the thermodynamic characterization of the fluids will undertake variations through the heat exchange process that could affect the determination of heat transfer coefficient. Therefore, the entire heat exchanges process should be discretized to various subdivisions. It is worth to mention that it is could be presumed which the properties of fluids remain unchanged in each subsection. The mean temperature difference approach is used to construct the heat exchangers and the heat exchangers employ tube-and-shell kind.

The heat transfer formula for each subdivision can be expressed as below:

$$Q_i = U_i A_i \Delta t_i \quad (13)$$

In which the mean temperature difference Δt_i employs the logarithmic mean temperature difference as follows:

$$\Delta t_i = \frac{(T_{f2,i+1} - T_{f1,i+1}) - (T_{f2,i} - T_{f1,i})}{\ln\left(\frac{T_{f2,i+1} - T_{f1,i+1}}{T_{f2,i} - T_{f1,i}}\right)} \tag{14}$$

The total heat transfer coefficient can be expressed as below:

$$\frac{1}{U_i} = \frac{1}{H_{f1}} + \frac{\delta}{\lambda} + \frac{1}{H_{f2}} \tag{15}$$

The influence of thermal resistance of pipe wall is neglected to make easier the computation, consequently the Eq. (15) can be written as follows:

$$\frac{1}{U_i} = \frac{1}{H_{f1}} + \frac{1}{H_{f2}} \tag{16}$$

The water flows in the shell and the CO_2 with supercritical pressure flows in the tube in the evaporator. The semi-empirical formulation of heat transfer coefficient of the geothermal water side which proposed by Petukhov [58] is employed as below:

$$U_w = 0.023\mathrm{Re}^{0.8}\mathrm{Pr}^{0.3}\frac{k_w}{D} \tag{17}$$

The semi-empirical formulation of heat transfer coefficient of the CO_2 side which proposed by Krasnoshchekov–Prototopov [59] is employed as below:

$$U_{CO_2} = \frac{k_{CO_2}}{D}\left[\frac{\frac{f_{bulk}}{8}\mathrm{Re}_{bulk}\overline{\mathrm{Pr}}}{12.7\left(\frac{f_{bulk}}{8}\right)^{0.5}(\mathrm{Pr}^{\frac{2}{3}}-1)+1.07}\right]\left[\frac{\overline{C_p}}{C_{pbulk}}\right]^{0.35} \times \left[\frac{K_{bulk}}{K_{wall}}\right]^{-0.33}\left[\frac{\mu_{bulk}}{\mu_{wall}}\right]^{-0.11} \tag{18}$$

It should be mentioned that the main assumption in the heater is that the environmental water flows in the shell and the natural gas with supercritical pressure flows in the tube. The two semi-empirical formulations of heat transfer coefficient are formulated as follow. The Eq. (16) is employed again on the water side and a semi-empirical equation proposed by Wang et al. [60] is used on the natural gas side as below:

$$U_{LNG} = 0.0156\mathrm{Re}_{bulk}^{0.82}\mathrm{Pr}_{bulk}^{0.5}\left(\frac{\rho_w}{\rho_{bulk}}\right)^{0.3}\left(\frac{\overline{C_p}}{C_{pbulk}}\right)^{0.4}\frac{K_{bulk}}{D} \tag{19}$$

The heat transfer process may consist of only a two phase heat transfer process or a two-phase and a single-phase heat transfer processes in the condenser, which is specified via the working fluid state at the turbine outlet. The main assumption is that that the CO_2 flows in the shell and the LNG under higher pressure flows in the tube. The Eq. (18) is employed on the LNG side, and the Cavallini and Zecchin equation [61] is employed for the two-phase region on the CO_2 side as following as:

$$U_{CO_2\text{-}TP} = 0.05\mathrm{Re}_{eq}^{0.8}\mathrm{Pr}_{liq}^{0.33}\frac{K_{liq}}{D} \tag{20}$$

In which the equivalent Reynolds Number can be defined as following as:

$$\mathrm{Re}_{eq} = \mathrm{Re}_{vap}\left(\frac{\mu_{vap}}{\mu_{liq}}\right)\left(\frac{\rho_{liq}}{\rho_{vap}}\right)^{0.5} + \mathrm{Re}_{liq} \tag{21}$$

$$\mathrm{Re}_{liq} = \frac{\dot{m}_f}{A_f}(1-x)\frac{D_w}{\mu_{sat.liq}} \tag{22}$$

$$\mathrm{Re}_{vap} = \frac{\dot{m}_f}{A_f}x\frac{D_w}{\mu_{sat.vap}} \tag{23}$$

Table 1
Parameters involved in the simulation of the geothermal power generation system.

Parameter	Unit	Value
Environment pressure	kPa	101.325
Environmental temperature	°C	25
Geothermal water temperature	°C	140
Pressure of Geothermal water	kPa	700
Geothermal water Mass flow rate	kg s^{-1}	10
Geothermal water Reinjection temperature	°C	85
Inlet temperature of CO_2 turbine	°C	120
Inlet pressure of CO_2 turbine	MPa	12
Isentropic efficiency of Turbine	%	80
Isentropic efficiency of Pump	%	70
Mass flow rate of LNG	kg s^{-1}	3.4
LNG inlet temperature	°C	−161.47
LNG pressure	kPa	101.4

The Eq. (16) is also employed for the single-phase area. The total heat exchange area of the system can be determined as follows:

$$A_{tot} = A_{evp} + A_{cnd} + A_{ht} \tag{24}$$

The system initial parameters are described in Table 1. As can be seen, the LNG initial temperature is −161.47 °C which is a typical available value. Also, the geothermal water enters the vapor generator at 140 °C.

3.2. Performance criteria

The exergy efficiency which is based on the second law of thermodynamics is employed to reflect the exploitation degree of the system energy consumption due to disability of the thermal efficiency of the system for reflecting the consumption level of the energy utilization by system. The exergy efficiency of the system is expressed as following as:

$$\eta_{exg} = \frac{W_{net}}{E_{in}} \tag{25}$$

in which E_{in} stands for the exergy input, comprising the exergy of LNG from the LNG storage tank and the underground geothermal water exergy.

Another assumption is that only the physical exergy is included, steady flowing fluid potential energy, macroscopic kinetic, and the chemical exergy are ignored. The exergy of steady flow can be written as below:

$$E_i = m[(h_i - h_0) - T_0(s_i - s_0)] \tag{26}$$

The exergy destruction of each equipment can be written as below as stated by the exergy balance equation. The equations were extracted based on Table 2.

For the evaporator:

$$I_{evp} = E_1 - E_2 + E_6 - E_3 \tag{27}$$

For the heater:

$$I_{ht} = E_9 - E_{12} + E_{10} - E_{11} \tag{28}$$

For the turbines:

$$I_{tb,CO_2} = E_3 - E_4 - W_{tb,CO_2} \tag{29}$$

$$I_{tb,NG} = E_{12} - E_{13} - W_{tb,NG} \tag{30}$$

Table 2
Exergy destruction rates of different investigated components.

Component	Exergy destruction rate
Heat exchanger	$I_{Hx} = \sum \dot{E}_{in} - \sum \dot{E}_{out}$
Turbine	$I_{tb} = \dot{E}_{in} - \dot{E}_{out} - \dot{W}_{ST}$
Condenser	$I_{cnd} = \sum \dot{E}_{in} - \sum \dot{E}_{out}$
Pump	$I_{Pump} = \dot{E}_{in} - \dot{E}_{out} + \dot{W}_{Pump}$

For the condenser:

$$I_{cnd} = E_4 - E_1 + E_8 - E_9 \quad (31)$$

For the pumps:

$$I_{PUMP,I} = E_5 - E_6 + W_{PUMP,I} \quad (32)$$

$$I_{PUMP,II} = E_7 - E_8 + W_{PUMP,II} \quad (33)$$

The total exergy loss is written as following equation:

$$I_{total} = I_{evp} + I_{ht} + I_{tb,CO_2} + I_{tb,NG} + I_{cnd} + I_{Pump,I} + I_{Pump,II} \quad (34)$$

ECOP (kW) of the cycle is formulated as below:

$$ECOP = \frac{W}{I_{total}} \quad (35)$$

3.3. Exergoeconomic analysis

Exergoeconomic analysis combines the exergy analysis and economic concepts to provide a set of useful information about cost of each stream which is crucial for optimized design of the system. To do this, first, an exergy analysis should be conducted on the plant. In the second step, an economic analysis is performed and finally the results of these two analyses are combined together. In the following, each of these analyses is described briefly.

3.3.1. Economic analysis

To perform the economic analysis, capital cost of all components should be calculated. Table 3 shows the equations used to calculate the capital cost of different components in the cycle.

3.3.2. Exergoeconomic balance

In performing exergoeconomic analysis, it is absolutely necessary to define the concept of fuel and product. For a control volume, fuel is the source of exergy which is consumed to generate the product and is different with actual fuel, such as natural gas, diesel, etc. Also the product is the desired result generated by using the fuel. Using the above definition, an exergoeconomic cost balance could be applied to each control volume as follows:

$$\dot{C}^Q + \sum \dot{C}_{in} + \dot{Z} = \dot{C}^W + \sum \dot{C}_{out} \quad (36)$$

$$\dot{C} = c\,\dot{E}x \quad (37)$$

where parameter $\dot{Z}$ is the investment cost rate which is computed as:

$$\dot{Z} = \frac{Z.CRF.\varphi}{H} \quad (38)$$

In this equation, Z is the capital cost of the component which is obtained using Table 3. H and φ are the total annual working hour and maintenance factor, respectively. Also *CRF* is the capital recovery factor that is defined as follows:

$$CRF = \frac{i(1+i)^N}{(1+i)^N - 1} \quad (39)$$

Table 3
Economic equations used in the model [6–10].

Component	Equation
Heat exchangers	$C_{HX} = (A_{HX}/0.093)^{0.78}$
Turbine	$\log C_{Turbine} = 2.6259 + 1.4398 \log(W) - 0.1776(\log(W))^2$
Pump	$\log C_{Pump} = 3.3892 + 0.0536 \log(W_{Pump}) + 0.1538(\log(W_{Pump}))^2$

Table 4
Constants used in economic analysis.

Parameter	Value
Working hour (h)	7446
Maintenance factor	1.06
Interest rate (%)	10
Plant life time (year)	20

In Eq. (39), i is the interest rate and N is the plant life time. The values of all economic parameters are represented in Table 4.

Using the above equations, exergoeconomic balances could be obtained. Table 5 lists the exergoeconomic balance of each component along with their auxiliary equations.

To perform a comparison in terms of exergoeconomic, several parameters are defined. The first two parameters are average cost per unit exergy of fuel and product which are defined as follows:

$$c_{F,k} = \frac{\dot{C}_{F,k}}{\dot{E}_{F,k}} \quad (40)$$

$$c_{P,k} = \frac{\dot{C}_{P,k}}{\dot{E}_{P,k}} \quad (41)$$

Relative cost difference of a component (r_k) is defined based on definition of average cost per unit exergy of fuel and product of the component.

$$r_k = \frac{c_{P,k} - c_{F,k}}{c_{F,k}} \quad (42)$$

This parameter represents the difference between the average cost of products and fuels which is due to the destruction and the investment cost.

The last two defined parameters are the cost flow rate associated with exergy destruction and the exergoeconomic factor which defined as follows:

$$\dot{C}_{D,k} = c_{F,k}\dot{E}_k^D \quad (43)$$

$$f_k = \frac{\dot{Z}_k}{\dot{Z}_k + \dot{C}_{D,k}} \quad (44)$$

where $\dot{C}_{D,k}$ is the cost of exergy destruction within each component and $\dot{Z}_k$ is the cost rate of all entering exergy streams supplemented with a component dependent cost rate. The exergoeconomic factor (f_k) is an indicator of relative importance of a component cost to the investment cost and the destruction cost associated with that component.

The exergoeconomic product cost rate of the cycle is formulated as below:

$$\sum C_P = \sum C_F + Z \quad (45)$$

Table 5
Exergoeconomic balances for each components.

Component	Cost rate balance	Auxiliary equation
Vapor generator	$\dot{C}_1 + \dot{C}_6 + \dot{Z}_{VG} = \dot{C}_2 + \dot{C}_3$	$\frac{\dot{C}_1}{\dot{E}_1} = \frac{\dot{C}_2}{\dot{E}_2}$
CO_2 Turbine	$\dot{C}_3 + \dot{Z}_{CO_2,tur} = \dot{C}_4 + \dot{C}_{CO_2,tur}$	$\frac{\dot{C}_3}{\dot{E}_3} = \frac{\dot{C}_4}{\dot{E}_4}$
Condenser	$\dot{C}_4 + \dot{C}_8 + \dot{Z}_{Cnd} = \dot{C}_9 + \dot{C}_5$	$\frac{\dot{C}_5}{\dot{E}_5} = \frac{\dot{C}_4}{\dot{E}_4}$
CO_2 Pump	$\dot{C}_5 + \dot{C}_{W,CO_2\ pump} + \dot{Z}_{CO_2\ pump} = \dot{C}_6$	$\frac{\dot{C}_{W,CO_2\ pump}}{\dot{W}_{CO_2\ pump}} = \frac{\dot{C}_{W,CO_2\ tur}}{\dot{W}_{CO_2\ tur}}$
LNG Pump	$\dot{C}_7 + \dot{C}_{W,LNG\ pump} + \dot{Z}_{LNG\ pump} = \dot{C}_8$	$\frac{\dot{C}_{W,CO_2\ pump}}{\dot{W}_{CO_2\ pump}} = \frac{\dot{C}_{W,LNG\ pump}}{\dot{W}_{LNG\ pump}}$
LNG heater	$\dot{C}_{10} + \dot{C}_9 + \dot{Z}_{Cnd} = \dot{C}_{11} + \dot{C}_{12}$	$\frac{\dot{C}_{10}}{\dot{E}_{10}} = \frac{\dot{C}_{11}}{\dot{E}_{11}}$
LNG Turbine	$\dot{C}_{12} + \dot{Z}_{LNG,tur} = \dot{C}_{13} + \dot{C}_{LNG,tur}$	$\frac{\dot{C}_{13}}{\dot{E}_{13}} = \frac{\dot{C}_{12}}{\dot{E}_{12}}$

3.4. Optimization process

The multi-objective optimization algorithm was used to optimize the power system to opt the system design variables. Moreover, Genetic algorithms (GA) employ stochastic and iterative search tool to determine optimal solution. The illustration of the MOEA is depicted through Fig. 3 [50–57].

The product cost rate ($\sum C_P$), the ecological coefficient of performance (*ECOP*) and the exergy efficiency (η_{exg}) are three objective functions for this work, which are identified by Eqs. (45), (35) and (25), respectively. Following parameters were selected as decision parameters:

T_3: turbine inlet temperature
p_3: turbine inlet pressure
p_4: Turbine back pressure
p_8: LNG Pressure

Furthermore, the below boundaries were considered to determine optimum values of the objective functions [62–64].

$$110 \leqslant T_3 \leqslant 127 \quad (46)$$

$$11 \leqslant p_3 \leqslant 16 \text{ Mpa} \quad (47)$$

$$0.8 \leqslant p_4 \leqslant 1.6 \text{ Mpa} \quad (48)$$

$$5 \leqslant p_8 \leqslant 10 \text{ Mpa} \quad (49)$$

In this work three efficient decision makers comprising Fuzzy, technique for order of preference by similarity to ideal solution (TOPSIS) and linear programming techniques for multidimensional analysis of preference (LINMAP) were used to opt the ultimate solution achieved from MOEA. The fully descriptions of the aforementioned method can be found in the Refs. [50–57].

4. Results and discussion

This study investigated a thermoeconomic analysis of a transcritical CO_2 cycle which is driven by an LNG process to absorb the heat duty of condenser and to produce further power. The results of steady state condition and state points are described in Table 6. As can be seen the LNG source has a temperature of −161.5 °C which is heated to −56 °C after condensation process of carbon dioxide. A pump is used to increase the pressure of liquefied natural gas from ambient pressure to 7 MPa in order to enter the condenser. It is further heated to 10 °C by producing the cold water at 5 which is beneficial for use in chillers. The geothermal source has a constant temperature of 140 °C and high pressure (700 kPa) which is cooled to 85 °C and at the returning point. The exergy of water at the inlet of heater is zero due to the ambient conditions. It is important to mention that the LNG releases some exergy when entering the condenser, although its temperature is increased. On the other hand, the CO_2 exergy is increased at the condenser.

Table 6
Thermodynamic properties of different state points of the cycle and the corresponding working fluids.

State point	Fluid type	T (°C)	p (MPa)	h (kJ/kg)	$\dot{m}$ (kg/s)	ex (kJ/kg)
1	Water	140	0.7	589.4	10	75.5
2	Water	85	0.665	356.5	10	22.9
3	CO_2	120	12	519.7	5.7	250
4	CO_2	−46	0.8	426.4	5.7	126.1
5	CO_2	−47.3	0.76	98.3	5.7	228.7
6	CO_2	−42.1	12.6	111.2	5.7	238.2
7	LNG	−161.5	0.101	0	3.4	1080
8	LNG	−158.5	7	20.5	3.4	1089.5
9	LNG	−56	6.65	572.3	3.4	680.4
10	Water	25	0.101	104.9	9.5	0
11	Water	5	0.101	21.1	9.5	2.9
12	LNG	10	6.318	806.4	3.4	623.5
13	LNG	−17.9	4	762.3	3.4	566.4

To investigate the system with respect to exergoeconomic criterion, the relative cost difference, exergoeconomic factor and other components are depicted in Table 7. The highest amount of exergy destruction occurs in condenser followed by vapor generator and CO_2 turbine. The highest value for condenser is due to large temperature difference between CO_2 fluid and LNG. According to thermoeconomic evaluation criteria, in designing a thermal system, much attention should be paid to components for which the sum of $\dot{Z} + \dot{C}_D$ is the highest. It is seen from Table 7 that CO_2 turbine and condenser have the highest rate of sum $\dot{Z} + \dot{C}_D$. After these components, LNG turbine and LNG pump have the next highest values. Therefore they are the most important components from the exergoeconomic point of view. The value of f indicates the relative importance of investment cost to destruction cost. Condenser has the lowest value of f among others and this shows that the costs associated to condenser comes almost exclusively from exergy destruction cost. On the other hand the value of 100% for vapor generator and LNG heater indicate that the exergy destruction cost is zero for these components which is expected due to free source of water inlet.

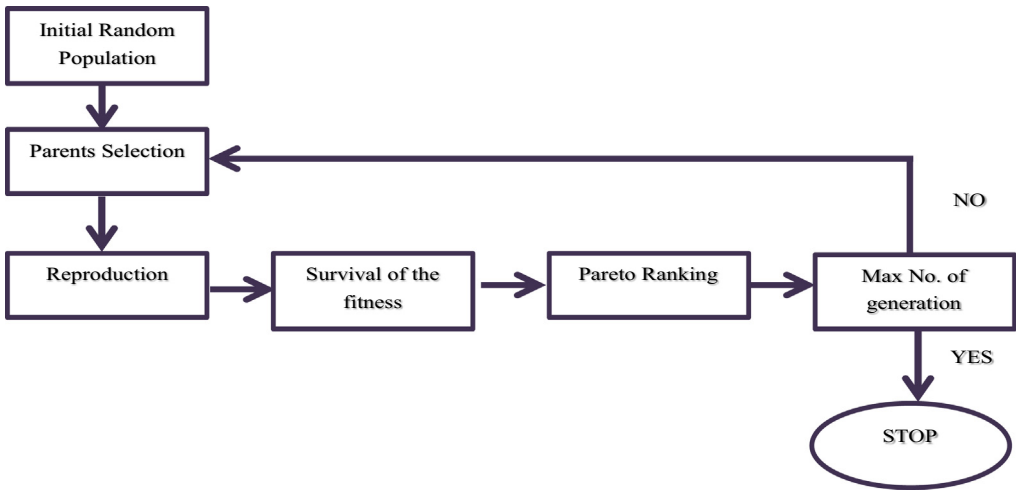

Fig. 3. Flow chart of multi-objective optimization algorithm [50–57].

Table 7
Exergoeconomic parameters of the integrated solar-ORC-LNG system.

Component	$c_F\left(\frac{\$}{GJ}\right)$	$c_P\left(\frac{\$}{GJ}\right)$	$\dot{E}^D$(kW)	$\dot{C}_D\left(\frac{\$}{year}\right)$	$\dot{Z}\left(\frac{\$}{year}\right)$	$\dot{Z}+\dot{C}_D\left(\frac{\$}{year}\right)$	f (%)	r (%)
Vapor Generator	1.8	0	458.4	0	3881.5	3881.5	100	Inf
CO_2 Turbine	23.5	15.9	174.5	87310	40132.1	127442.1	31.5	47.9
Condenser	15.9	6.5	802.3	165685.1	6042.3	171727.4	3.5	142.3
CO_2 Pump	33.4	23.5	19.5	14461.1	2502.2	16963.3	14.8	42.3
LNG Pump	52.5	23.5	36.8	27249.4	2405.6	29654.9	8.1	123.8
Heater	0.9	0	165	0	5216.9	5216.9	100	Inf
LNG Turbine	23.5	14.9	44	20724.3	19479.7	40204	48.5	57.1

The value of r is the relative cost difference and this difference is because of capital investment and exergy destruction costs. Therefore lower values of r are preferable. Infinite values of r for vapor generator and LNG heater are due to the zero cost of fuel. Condenser and LNG heater have the highest value of r which is due to high exergy destruction cost.

LNG turbine has the third highest f value and relatively high value for relative cost difference (r) compared to other components. Therefore, if the $\dot{Z}$ value for LNG turbine is reduced, the cost effectiveness of the entire system will improve.

4.1. Effect of turbine inlet pressure

Fig. 4 shows the influence of inlet pressure of CO_2 turbine on exergy efficiency of the system. The exergy input keeps constant because the mass flow rate of the LNG and geothermal water are not varied in this system. Moreover, similar trend as the net power output of the system was observed for the exergy efficiency of the system. On the other hand, an opposite trend is seen for the product cost rate of the system in a way that there is an optimum minimum working condition for it. The minimum point for the product cost rate lags behind the maximum efficiency. This behavior makes the optimization process a necessary part to find the best optimal working condition with respect to both highest efficiency and minimum product cost rate.

Fig. 5 depicts the influence of inlet pressure of CO_2 turbine on the system output power. By increasing the inlet pressure of CO_2 turbine the power consumption of pump II and power output of NG turbine kept constant. The main reason is that the inlet pressure of CO_2 turbine is not effective on the pump II and the NG turbine. By increasing the inlet pressure of CO_2 turbine the mass flow rate of CO_2 increased consequently. By increasing the inlet pressure of CO_2 turbine the output power of CO_2 turbine increased, since the changing of the mass flow rate of CO_2 is higher than that of the enthalpy changing through CO_2 turbine. An increasing the inlet pressure of CO_2 turbine results an increase in the power consumption of pump I. Owing to the mutual influence of the power consumption of pump I and the power output of CO_2 turbine, the net power output increased firstly, achieving a highest value, and finally decreased. Also, the variation of the ecological coefficient

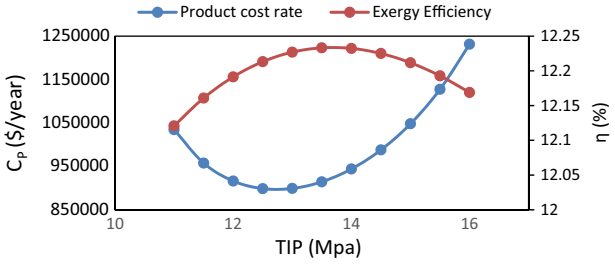

Fig. 4. Variation of turbine inlet pressure on product cost rate and exergy efficiency of the system.

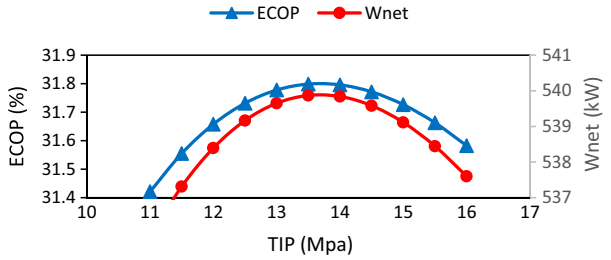

Fig. 5. Variation of ecological coefficient of performance and output power with turbine inlet pressure.

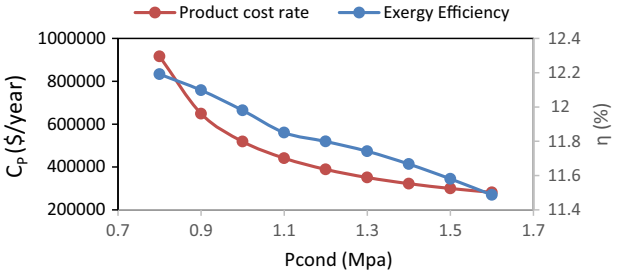

Fig. 6. Variation of condensate pressure on product cost rate and exergy efficiency of the system.

of performance of the system versus the vapor generator pressure is seen in Fig. 5. The ECOP of the system follows the similar trend as the net output power of the system.

4.2. Effect of condensate pressure

Fig. 6 shows the effect of condensate pressure on exergy efficiency and product cost rate. Unlike the previous case in which both exergy efficiency and product cost rate had an optimum value, in this case both these parameters show a downward trend. As can be seen, the product cost rate shows a decreasing trend with condensation pressure mainly due to the decrease in work output and size of heat exchangers which contributes to lower capital cost

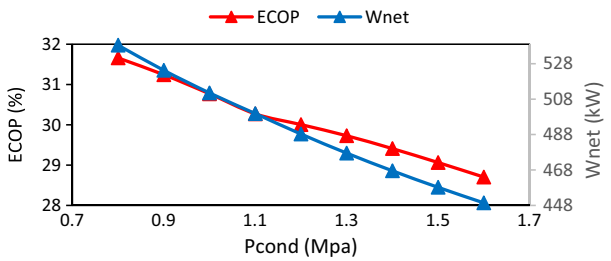

Fig. 7. Variation of ECOP and output power with condensate pressure.

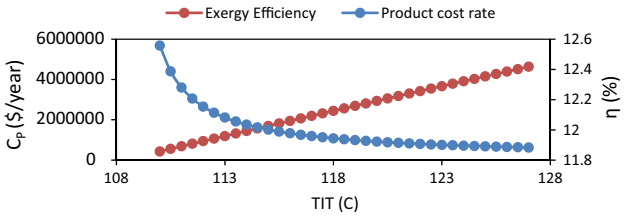

Fig. 8. Effect of turbine inlet temperature on product cost rate and exergy efficiency of the system.

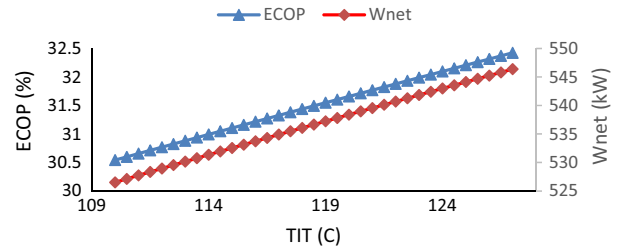

Fig. 9. Variation of ECOP and output power with turbine inlet temperature.

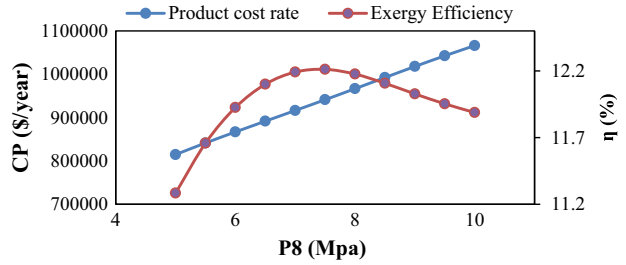

Fig. 10. Effect of LNG pressure on product cost rate and exergy efficiency of the system.

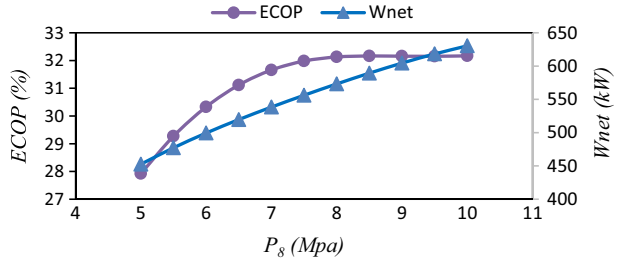

Fig. 11. Variation of ECOP and output power with LNG pressure.

of the system. Also, the figure illustrates that the Exergy efficiency is decreased noticeably by increasing the condensate pressure which is mainly due to lower work output when the heat input is fixed.

Fig. 7 shows the variation of ecological coefficient of performance along with work output with condensate pressure. As mentioned before, the increased condensate pressure has a direct effect on work output and decreases it. Also, the Fig. 7 illustrates that the ECOP is decreased noticeably by increasing the CO_2 turbine back pressure (P_4). By increasing the CO_2 turbine back pressure, the enthalpy change through CO_2 turbine considerably decreases which causes the power output of CO_2 turbine to decrease. By increasing the back pressure of CO_2 turbine the CO_2 mass flow rate generated in evaporator is increased. This is owing to the decreasing in the heat absorption of unit CO_2 mass flow rate. Consequently, the power consumption of pump I is increased. The power consumption and the output power of NG turbine and of pump II remain constant. As a result, by increasing the back pressure of CO_2 turbine the net power output of the system is decreased. Accordingly, by reducing the net power output, the ECOP is also reduced.

4.3. Effect of turbine inlet temperature

Fig. 8 illustrates the effect of turbine inlet temperature on exergy efficiency and product cost rate. It is shown that increasing the inlet temperature has a positive effect on reduction of product cost rate which is mainly due to lower exergy destruction rates and lower exergy cost, although it causes higher work output and higher heat exchanger sizes which contributes to higher capital investments. As it can be seen, it has the highest impact on the product cost rate and when the turbine inlet temperature decreases from 128 °C to 110 °C, its product cost rate increases from 600,000 $/year to almost 6 million dollars per year. Also, the Fig. 8 depicts the influence of CO_2 turbine inlet temperature on exergy efficiency of the system. The exergy efficiency of the system is increased by increasing the inlet temperature of CO_2 turbine as demonstrated in Fig. 8. The main reason behind that is when turbine inlet temperature increases; it means that more exergy is extracted from the same hot geothermal water and as a result total output power of the cycle increases as shown in Fig. 9.

Fig. 9 shows the effect of CO_2 turbine inlet temperature on *ECOP* of the system. The *ECOP* of the system is increased by increasing the inlet temperature of CO_2 turbine as shown in the figure. Furthermore, similar trend as the net power output of the system was observed for *ECOP* of the system.

4.4. Effect of LNG pressure

The effect of LNG pressure on exergy efficiency, product cost rare, ECOP and net work is illustrated in Figs. 10 and 11. Fig. 10

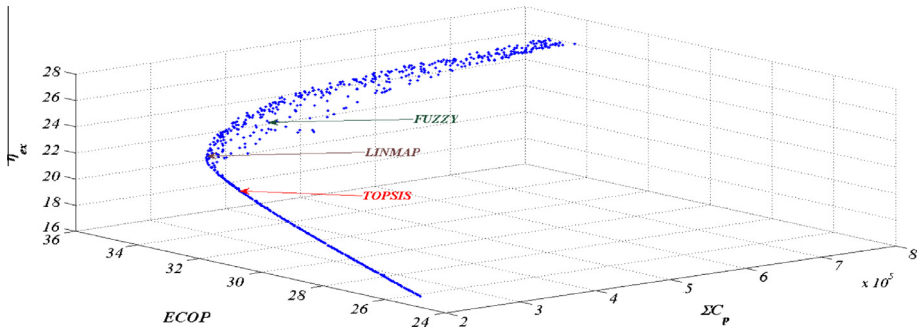

Fig. 12. Pareto optimal frontier in the objectives' space.

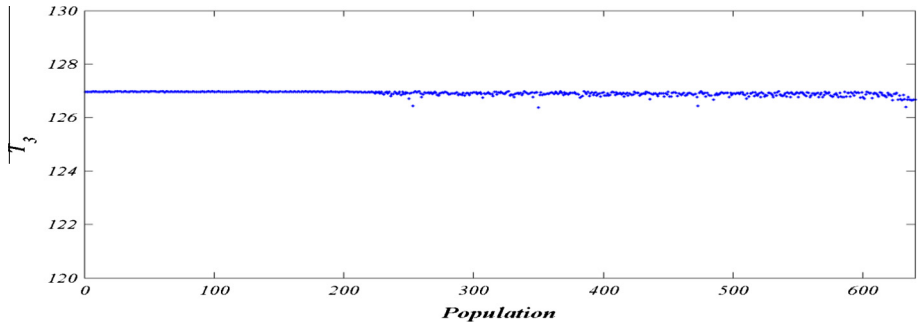

Fig. 13. The changes of T_3 for the optimal points on Pareto front.

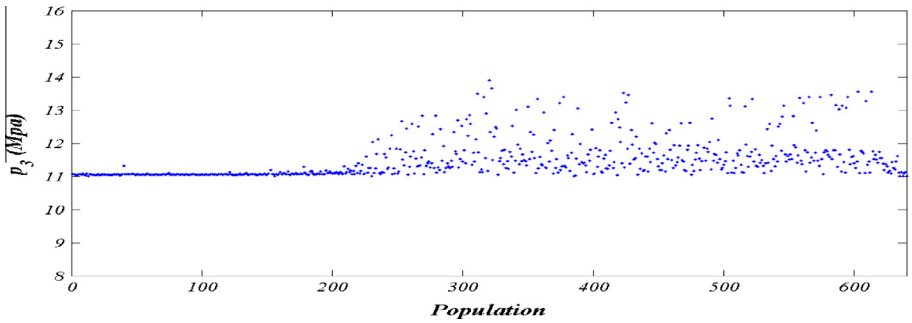

Fig. 14. The changes of p_3 for the optimal points on Pareto front.

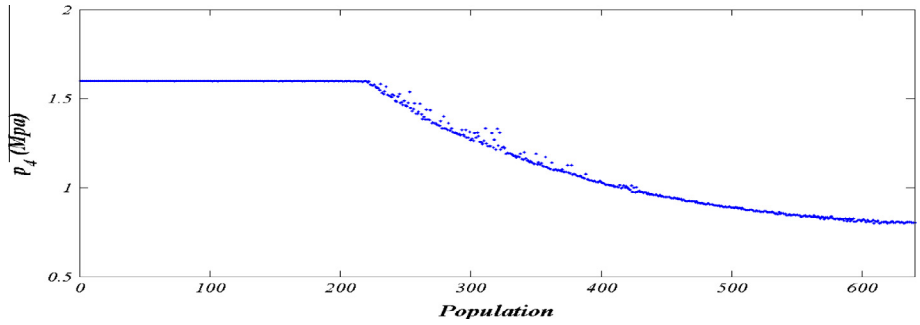

Fig. 15. The changes of p_4 for the optimal points on Pareto front.

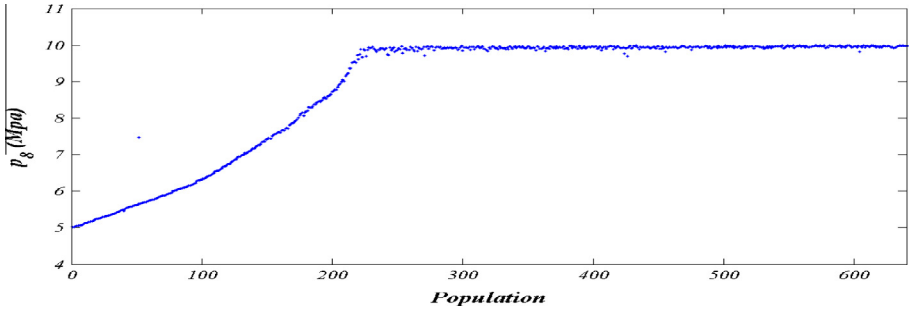

Fig. 16. The changes of p_8 for the optimal points on Pareto front.

shows that there is optimum exergy efficiency in the system. The net power produced by the LNG expander is very sensitive to LNG pressure produced by the pump and increasing the pressure increases the power produced by the expander. This trend is shown in Fig. 11 which the net power is increased while the CO_2 turbine work output is fixed due to constant parameters of CO_2 cycle. However, the exergy input to the system is also increased because the LNG process exergy should be taken into account when calculating the exergy efficiency. The net effect is that by increasing the LNG pressure the both the work output and exergy input to the system is increased in a way that their proportion (exergy efficiency) is increased firstly and then increase in LNG exergy is more than enhanced power output resulting in decrement of exergy efficiency of the system. However, a linear trend is seen for the product cost rate which is due to linear increment of work output shown in Fig. 11. It is worth mentioning that in

Table 8
Decision making of multi-objective optimal solutions for this system.

Decision making method	Decision variables				Objectives			Index deviation
	T_3	p_3	p_4	p_8	*ECOP*	η_{exg}	C_P	
TOPSIS	126.970	11.116	1.599	8.154	32.165	20.500	263592.149	0.074
LINMAP	126.878	11.137	1.516	9.918	33.999	22.104	295001.264	0.132
Fuzzy	126.972	12.337	1.235	9.90	33.869	23.966	370378.758	0.270
Ideal solution	–	–	–	–	35.295	27.465	223151.894	0
Non-ideal solution	–	–	–	–	25.405	16.372	768094.1673	∞

Table 9
Error analysis based on the mean absolute percent error (MAPE) method for this system.

Decision making method	TOPSIS			LINMAP			Fuzzy		
Objectives	*ECOP*	η_{exg}	C_P	*ECOP*	η_{exg}	C_P	*ECOP*	η_{exg}	C_P
Max error (%)	0.262	0.278	0.697	0.256	0.319	0.799	0.123	0.191	0.699
Average error (%)	0.185	0.193	0.478	0.178	0.177	0.505	0.096	0.091	0.403

all previous cases, ECOP had a trend similar to net output power, but in this case its variation is close to the variation of exergy efficiency. This is mostly because that natural gas has a key role in exergy efficiency and destruction of the plant, as it is one of the two sources of inlet exergy into the system and a small variation in its condition can considerably change the exergy destruction of the plant.

5. Optimization results

Here, optimization results are shown based on four decision variables including turbine inlet pressure, turbine inlet temperature, Turbine back pressure and LNG Pressure which have dominant effect on the total system.

Pareto optimal frontier for three objective functions, objective function associated to the product cost rate ($\sum C_P$), the ecological coefficeint of performance (*ECOP*) and the exergy efficiency (η_{exg}) of the system are represented in Fig. 12.

Figs. 13–16 demonstrate the changes of decision parameters' values in their acknowledged range for the optimal design points on the Pareto frontier. The changes of the T_3 parameter is depicted through Fig. 13.

Fig. 14 shows that, the changes of p_3 values for the optimal design points on the Pareto frontier varies from 11 to 13.9. Fig. 15 depicts that, the changes of p_4 values for the optimal design points on the Pareto frontier varies from 0.8 to 1.6. The changes of p_8 values for the optimal design points on the Pareto frontier is demonstrated through Fig. 16.

Table 8 illustrates the optimal outputs obtained for objective functions and decision parameters by running TOPSIS, Fuzzy and LINMAP methods for this optimization process. Table 8 reports the values of objective functions and decision variables for the selected answers introduced into each arrangement. To have better understanding for the answers achieved here compared to the deviation of each answer from the non-ideal and ideal answers are determined as follow:

$$d_+ = \sqrt{\left(\sum C_P - \sum C_{P,n}\right)^2 + (ECOP - ECOP_n)^2 + (\eta_{exg} - \eta_{exg,n})^2} \tag{50}$$

$$d_- = \sqrt{\left(\sum C_P - \sum C_{P,n,non\text{-}ideal}\right)^2 + (ECOP - ECOP_{n,non\text{-}ideal})^2 + (\eta_{exg} - \eta_{exg,n,non\text{-}ideal})^2} \tag{51}$$

$$d = \frac{d_+}{(d_+) + (d_-)} \tag{52}$$

$\sum C_P$, *ECOP* and η_{exg}, denote Euclidian the product cost rate ($\sum C_P$), the ecological coefficeint of performance (*ECOP*) and the exergy efficiency (η_{exg}). Moreover, Table 8 comprises the deviation index (d) for the answer obtained from each decision maker in the last column.

The indexes of deviation for the MOEA of the present work are 0.074, 0.132 and 0.270 for answers achieved employing the TOPSIS, LINMAP and Fuzzy decision makers, correspondingly. Furthermore, the last column of Table 8 points out that the TOPSIS decision-maker has a lowest deviation index in comparison with other decision makers; consequently the answer which is chosen via the TOPSIS decision-maker is considered as a final optimal answer of the MOEA for this work.

To appraise accuracy of each decision makers for determining the optimal objectives' values, mean absolute percentage error (MAPE) analysis was carried out.

Table 9 reports MAAE (Maximum Absolute Percentage Error) of the decision makers employed in this study. Besides,

Table 9 summarized the MAPE values of the decision makers.

6. Conclusions

This work made attempt to present the exergoeconomic analysis of a transcritical CO_2 geothermal power generation system via the cold energy exploitation of LNG. It is assumed that the system works under steady state conditions to develop the mathematical approach and simulate the system. The effects of four main thermodynamic parameters including inlet temperature of CO_2 turbine, inlet pressure of CO_2 turbine, back pressure of CO_2 turbine and LNG pressure on the performance of the system including product cost rate and exergy efficiency was systematically studied. To drop the back pressure of the CO_2 turbine, LNG is employed as the heat sink in the transcritical CO_2 geothermal power generation system, which results in positive effects such as increasing the output power of the CO_2 turbine by allowance of lower back pressure and further power generation via the NG turbine itself. Exergoeconomic analysis

reveals that CO_2 turbine and condenser have the highest rate of sum $\dot{Z} + \dot{C}_D$ and special attention should be paid to these components. Also, there is room for improvement of LNG turbine with respect to its relatively high value of r. Besides, the condenser and LNG heater have the highest value of r which are due to the high exergy destruction cost. Parametric analysis was performed to investigate the effect of four key parameters on the system including the CO_2 turbine inlet pressure and temperature along with condensate pressure and LNG pressure. It is seen that the cumulative effect of these parameters on the system is high which makes the optimization process necessary for this system. An optimization process was done and via three decision making techniques the optimal values were presented. The results show that there is significant variation in optimal point based on three different decision making techniques.

References

[1] Ashouri M, Astaraei FR, Ghasempour R, Ahmadi M, Feidt M. Thermodynamic and economic evaluation of a small-scale organic Rankine cycle integrated with a concentrating solar collector. Int J Low-Carbon Technol 2015:ctv025.
[2] DiPippo R. Second law assessment of binary plants generating power from low – temperature geothermal fluids. Geothermics 2004;33:565–86.
[3] Tchanche BF, Lambrinos G, Frangoudakis A, Papadakis G. Low-grade heat conversion into power using organic Rankine cycles – a review of various applications. Renew Sustain Energy Rev 2011;15:3963–79. 10.
[4] Saleh B, Koglbauer G, Wendland M, Fischer J. Working fluids for low temperature organic Rankine cycles. Energy 2007;32:1210–21.
[5] Maizza V, Maizza A. Working fluids in non-steady flows for waste energy recovery systems. Appl Thermal Energy 1996;16(7):579–90.
[6] Badr O, Probert SD, O'Callaghan PW. Selecting a working fluid for a Rankine-Cycle Engine. Appl Energy 1985;21:1–42.
[7] Hettiarachchia HDM, Golubovica M, Worek WM, Ikegami Y. Optimum design criteria for an organic Rankine cycle using low-temperature geothermal heat sources. Energy 2007;32:1698–706.
[8] Drescher U, Brüggemann D. Fluid selection for the organic Rankine cycle (ORC) in biomass power and heat plants. Appl Therm Eng 2007;27:223–8.
[9] Yamamoto T, Furuhata T, Arai N, Mori K. Design and testing of the organic Rankine cycle. Energy 2001;26:239–51.
[10] Shengjun Zh, Huaixin W, Tao G. Performance comparison and parametric optimization of subcritical organic Rankine cycle (ORC) and transcritical power cycle system for low-temperature geothermal power generation. Appl Energy 2011;29:2740–54.
[11] Kalina AI. Combined cycle system with novel bottoming cycle. ASME J Eng Gas Turb Power 1984;106:737–42.
[12] El-Sayed YM, Tribus M. Theoretical comparison of Rankine and Kalina cycles. ASME Adv Energy Syst Div 1985:97–102.
[13] Ashouri Milad, Vandani Amin Mohammadi Khoshkar, Mehrpooya Mehdi, Ahmadi Mohammad H, Abdollahpour Amir. Techno-economic assessment of a Kalina cycle driven by a parabolic Trough solar collector. Energy Convers Manage 2015;105:1328–39.
[14] Marston CH. Parametric analysis of the Kalina cycle. ASME J Eng Gas Turb Power 1990;112:107–16.
[15] Rogdakis ED. Thermodynamic analysis, parametric study and optimum operation of the Kalina cycle. Int J Energy Res 1994;20:359–70.
[16] Marston CH. Gas turbine bottoming cycles: triple-pressure steam versus Kalina. ASME J Eng Gas Turb Power 1995;117:10–5.
[17] Nag PK, Gupta A. Exergy analysis of the Kalina cycle. Appl Therm Eng 1998;18:427–39.
[18] Zamfirescu C, Dincer I. Thermodynamic analysis of a novel ammonia-water trilateral Rankine cycle. Thermochim Acta 2008;447:7–15.
[19] Fischer J. Comparison of trilateral cycles and organic Rankine cycles. Energy 2011;36:6208–19.
[20] Quick H, Michael J, Arslan U, Huber H. Geothermal application in low-enthalpy regions. Renew Energy 2013;49:133–6.
[21] Hung T. Waste heat recovery of organic Rankine cycle using dry fluids. Energy Convers Manage 2001;42:539–53.
[22] Nguyen TQ, Slawnwhite JD, Boulama KG. Power generation from residual industrial heat. Energy Convers Manage 2010;51:2220–9.
[23] Chen H, Yogi Goswami D, Rahman MM, Stefanakos EK. Energetic and exergetic analysis of CO2- and R32-based transcritical Rankine cycles for low-grade heat conversion. Appl Energy 2011;88:2802–8.
[24] Walraven D, Laenen B, D'haeseleer W. Comparison of thermodynamic cycles for power production from low-temperature geothermal heat sources. Energy Convers Manage 2013;66:220–33.
[25] Velez F, Segovia J, Chejne F, Antolín G, Quijano A, Carmen Martín M. Low temperature heat source for power generation: exhaustive analysis of a carbon dioxide transcritical power cycle. Energy 2011;36:5497–507.
[26] Wang J, Sun Z, Dai Y, Ma S. Parametric optimization design for supercritical CO_2 power cycle using genetic algorithm and artificial neural network. Appl Energy 2010;87:1317–24.
[27] Baik YJ, Kim M, Chang KC, Kim SJ. Power-based performance comparison between carbon dioxide and R125 transcritical cycles for a low-grade heat source. Appl Energy 2011;88:892–8.
[28] Lin W, Huang M, He H, Gu A. A transcritical CO2 rankine cycle with LNG cold energy utilization and liquefaction of CO2 in gas turbine exhaust. J Energy Resour Technol 2009;131:042201.
[29] Gao T, Lin W, Gu A. Improved processes of light hydrocarbon separation from LNG with its cryogenic energy utilized. Energy Convers Manage 2011;52:2401–4.
[30] Mehrpooya M, Kalhorzadeh M, Chahartaghi M. Investigation of novel integrated air separation processes, cold energy recovery of liquefied natural gas and carbon dioxide power cycle. J Clean Prod 2016;113:411–25.
[31] Wang J, Yan Z, Wang M, Dai Y. Thermodynamic analysis and optimization of an ammonia-water power system with LNG (liquefied natural gas) as its heat sink. Energy 2013;50:513–22.
[32] Song Y, Wang J, Dai Y, Zhou E. Thermodynamic analysis of a transcritical CO_2 power cycle driven by solar energy with liquefied natural gas as its heat sink. Appl Energy 2012;92:194–203.
[33] Esen Hikmet, Inalli Mustafa, Esen Mehmet. Technoeconomic appraisal of a ground source heat pump system for a heating season in eastern Turkey. Energy Convers Manage 2006;47(9):1281–97.
[34] Esen Hikmet, Inalli Mustafa, Esen Mehmet, Pihtili Kazim. Energy and exergy analysis of a ground-coupled heat pump system with two horizontal ground heat exchangers. Build Environ 2007;42(10):3606–15.
[35] Esen Hikmet, Inalli Mustafa, Esen Mehmet. A techno-economic comparison of ground-coupled and air-coupled heat pump system for space cooling. Build Environ 2007;42(5):1955–65.
[36] Temir G, Bilge D. Thermoeconomic analysis of a trigeneration system. Appl Therm Eng 2004;24:2689–99.
[37] Kong XQ, Wang RZ, Huang XH. Energy efficiency and economic feasibility of CCHP driven by stirling engine. Energy Convers Manage 2004;45:1433–42.
[38] Huangfu Y, Wu JY, Wang RZ, Kong XQ, Wei BH. Evaluation and analysis of novel micro-scale combined cooling, heating and power (MCCHP) system. Energy Convers Manage 2007;48:1703–9.
[39] Mehrpooya Mehdi, Ansarinasab Hojat. Exergoeconomic evaluation of single mixed refrigerant natural gas liquefaction processes. Energy Convers Manage 2015;99:400–13.
[40] Balli O, Aras H, Hepbasli A. Thermodynamic and thermoeconomic analyses of a trigeneration (TRIGEN) system with a gas–diesel engine: Part II – An application. Energy Convers Manage 2010;51:2260–71.
[41] Al-Sulaiman FA, Dincer I, Hamdullahpur F. Thermoeconomic optimization of three trigeneration systems using Organic Rankine Cycles: Part I – Formulations. Energy Convers Manage 2013;69:199–208.
[42] Al-Sulaiman FA, Dincer I, Hamdullahpur F. Thermoeconomic optimization of three trigeneration systems using Organic Rankine Cycles: Part II–applications. Energy Convers Manage 2013;69:209–16.
[43] Mehrpooya Mehdi, Ansarinasab Hojat. Advanced exergoeconomic evaluation of single mixed refrigerant natural gas liquefaction processes. J Nat Gas Sci Eng 2015;26:782–91.
[44] Mehrpooya Mehdi, Ansarinasab Hojat. Advanced exergoeconomic analysis of the multistage mixed refrigerant systems. Energy Convers Manage 2015;103:705–16.
[45] Özyer T, Zhang M, Alhajj R. Integrating multi-objective genetic algorithm based clustering and data partitioning for skyline computation. Appl Intell 2011;35:110–22.
[46] Beatrice O, Brian JR, Franklin H. Multi-objective genetic algorithms for vehicle routing problem with time windows. Appl Intel 2006;24:17–30.
[47] Blecic I, Cecchini A, Trunfio G. A decision support tool coupling a causal model and a multi-objective genetic algorithm. Appl Intell 2007;26:125–37.
[48] Veldhuizen DAV, Lamont GB. Multi objective evolutionary algorithms analyzing the state-of-the-art. Evol Comput 2000;8(2):125–47.
[49] Konak A, Coit DW, Smith AE. Multi-objective optimization using genetic algorithms: a tutorial. Reliab Eng Syst Safety 2006;91:992–1007.
[50] Ahmadi MH, Hosseinzade H, Sayyaadi H, Mohammadi AH, Kimiaghalam F. Application of the multi-objective optimization method for designing a powered Stirling heat engine: design with maximized power, thermal efficiency and minimized pressure loss. Renew Energy 2013;60:313–22.
[51] Ahmadi MH, Sayyaadi H, Mohammadi AH, Barranco-Jimenez A Marco. Thermo-economic multi-objective optimization of solar dish-Stirling engine by implementing evolutionary algorithm. Energy Convers Manage 2013;73:370–80.
[52] Ahmadi MH, Dehghani S, Mohammadi AH, Feidt M, Barranco-Jimenez A Marco. Optimal design of a solar driven heat engine based on thermal and thermo-economic criteria. Energy Convers Manage 2013;75:635–42.
[53] Ahmadi MH, Ahmadi MA, Bayat R, Ashouri M, Feidt M. Thermo-economic optimization of Stirling heat pump by using non-dominated sorting genetic algorithm. Energy Convers Manage 2015;91:315–22.
[54] Sayyaadi Hoseyn, Ahmadi Mohammad Hossein, Dehghani Saeed. Optimal design of a solar-driven heat engine based on thermal and ecological criteria. J Energy Eng 2014. http://dx.doi.org/10.1061/(ASCE)EY.1943-7897.0000191. 04014012.
[55] Ahmadi MH, Ahmadi MA, Mehrpooya M, Sameti M. Thermo-ecological analysis and optimization performance of an irreversible three-heat-source absorption heat pump. Energy Convers Manage 2015;90:175–83.
[56] Sadatsakkak Seyed Abbas, Ahmadi Mohammad Hossein, Ahmadi Mohammad Ali. Thermodynamic and thermo-economic analysis and optimization of an irreversible regenerative closed Brayton cycle. Energy Convers Manage 2015;94:124–9.

[57] Sadatsakkak Seyed Abbas, Ahmadi Mohammad H, Bayat Roham, Pourkiaei Seyed Mohsen, Feidt Michel. Optimization density power and thermal efficiency of an endoreversible Braysson cycle by using non-dominated sorting genetic algorithm. Energy Convers Manage 2015;93:31–9.
[58] Incropera FP, Dewitt DP. Fundamentals of heat and mass transfer. 5th ed. New York: John Wiley and Sons; 2002.
[59] Angelino G, Invernizzi CM. Carbon dioxide power cycles using liquid natural gas as heat sink. Appl Therm Eng 2009;29:2935–41.
[60] Wang YZ, Hua YX, Meng H. Numerical studies of supercritical turbulent convective heat transfer of cryogenic-propellant methane. J Thermophys Heat Transfer 2010;24:490–500.
[61] Cavallini A, Zecchin R. A dimensionless correlation for heat transfer in forced convection condensation. In: Proceedings of the fifth international heat transfer conference. p. 309–13.
[62] Xia Guanghui, Qingxuan Sun Xu, Cao Jiangfeng Wang, Yizhao Yu, Wang Laisheng. Thermodynamic analysis and optimization of a solar-powered transcritical CO_2 (carbon dioxide) power cycle for reverse osmosis desalination based on the recovery of cryogenic energy of LNG (liquefied natural gas). Energy 2014;66:643–53.
[63] Song Yuhui, Wang Jiangfeng, Dai Yiping, Zhou Enmin. Thermodynamic analysis of a transcritical CO_2 power cycle driven by solar energy with liquified natural gas as its heat sink. Appl Energy 2012;92:194–203.
[64] Wang Jianyong, Wang Jiangfeng, Dai Yiping, Zhao Pan. Thermodynamic analysis and optimization of a transcritical CO_2 geothermal power generation system based on the cold energy utilization of LNG. Appl Therm Eng 2014;70(1):531–40.